All-Dry Synthesis of Single Crystal NMC Cathode Materials for Li-Ion Batteries

Journal of The Electrochemical Society, 2020 **167** 130536

All-Dry Synthesis of Single Crystal NMC Cathode Materials for Li-Ion Batteries

Lituo Zheng,[1,*] J. Craig Bennett,[2] and M. N. Obrovac[1,3,,z]**

[1]*Department of Chemistry, Dalhousie University, Halifax, NS B3H 4R2, Canada*
[2]*Department of Physics, Acadia University, Wolfville, NS B4P 2R6, Canada*
[3]*Department of Physics and Atmospheric Science, Dalhousie University, Halifax, NS B3H 4R2, Canada*

Single crystal (SC) cathode materials with a layered structure are considered to be state-of-the-art for lithium ion batteries. However, their production involves many steps and can produce large amounts of wastewater. Here we report an all-dry method for making SC cathode materials, with $LiNi_{0.6}Mn_{0.2}Co_{0.2}O_2$ (SC-NMC) used as a specific example. It was found that a SC-NMC precursor in the form of a previously unobserved rock-salt (Ni, Mn, Co)O solid solution phase can be made phase pure by ball milling. This demonstrates that precursors with atomic scale mixing can be achieved by dry methods. It is furthermore shown that large precursor particle sizes are not necessary to form large SC-NMC particles, as is commonly believed. Instead, large crystallites could just as easily be made from submicron precursors by adjusting the sintering time in air. As a result, highly crystalline SC-NMC with precisely controlled average crystallite sizes ranging from ~2–10 μm could be made from submicron precursor powders made using an all-dry process.

 [DOI: 10.1149/1945-7111/abbcb1]

Manuscript submitted June 16, 2020; revised manuscript received September 25, 2020. Published October 8, 2020.

Supplementary material for this article is available online

As lithium ion batteries continue to expand in use in applications such as electric vehicles, there are increasing demands for higher energy density and longer life batteries with emphasis on decreasing cost while simultaneously reducing waste and the environmental impacts of battery production.[1] Single crystal (SC) cathode materials with layered structures, such as single crystal $LiNi_xMn_yCo_zO_2$ (SC-NMC) have recently gained the spotlight as promising materials for high-performance Li-ion batteries.[2–4] Single crystal cathode materials are characterized by having particles composed of one or a few large grains (2–10 μm) in contrast to conventional polycrystalline materials, which are usually spherical aggregates of many small submicron crystallites.[2] Particle cracking in polycrystalline cathode materials is one of their more common failure mechanisms, leading to isolated active materials (capacity loss via electrical connection), and increased surface area (capacity loss via surface reactions with electrolyte).[5,6] This is especially pronounced in nickel-rich NMC materials ($LiNi_xMn_yCo_zO_2$ where $x \geqslant 0.6$).[5] Nickel-rich NMC materials are gaining more market share as they can deliver high energy density with reduced cost.[7] One challenge is that high nickel materials suffer from poor cycling performance as a result of large volume changes during cycling.[5] The use of SC-NMC can effectively improve cycling performance. It has been reported that compared to conventional polycrystalline NMC, SC-NMC has reduced particle cracking during cycling, due to the structural integrity and the uniform contraction/expansion of each crystallite.[8] In addition, reduced electrolyte reactivity and gas production at the cathode surface has been reported for SC NMC, leading to batteries projected to have lifetimes sufficient to power vehicles for over a million miles (1.6 million kilometers).[9]

In commercial lithium ion batteries, both polycrystalline and single crystal cathode materials are synthesized from co-precipitated precursors made using a continuous stirred-tank reactor, as illustrated schematically in Fig. S1 (available online at stacks.iop.org/JES/167/130536/mmedia).[2,3] This process requires accurate control of concentration, temperature, feeding rate, pH, stirring intensity, etc.[10] The resulting product can have a high sulfur content, requiring it to be repeatedly washed, filtered, and dried.[11] Even though it is a relatively mature process, it is still costly, consumes large amounts of energy and water, and produces wastewater and chemical waste.[12] It is also limited by the co-precipitation chemistry. For example, aluminum substitution is an effective way to enhance the cathode performance, however, it is difficult to prepare aluminum-containing precursor due to the tendency of the Al^{3+} ion to form double hydroxides in solution.[13] Recent developments also involve using higher oxidation state elements, such as tungsten, in cathode materials.[14] This will pose more challenges for co-precipitation synthesis.

A main reason why co-precipitation is used in the commercial production of SC-NMC is because of its ability to make precursors in which the constituent metal elements are mixed at an atomic scale, facilitating the even diffusion and the formation of desired lithiated product during sintering.[10] Without such fine mixing of the constituent elements, multiphase materials can form instead of the desired phase-pure product. However, ball-milling or mechanochemical synthesis has been successfully used to prepare precursors for $LiMO_2$ (M = Ti, Mn and Fe) and $Li_xMn_2O_4$ cathode materials.[15,16] Recently, we have shown that commercial-quality NMC cathode powder can be made from microgranulated ball milled precursors, prepared from metal oxide feedstocks.[17] These precursors were made with no waste at 100% yield. The resulting cathode powder was phase-pure and even had similar shape and particle size distribution as typical commercial NMC cathode powder made by co-precipitation.[17] Therefore, dry methods present attractive alternatives to co-precipitation.

Another reason why co-precipitation is used in the commercial production of SC-NMC is that it produces monodisperse particles having the low surface area and size desired of the product SC-NMC particles.[18] As mentioned above, such qualities can also be achieved by microgranulated ball milled precursors.[17] However, considering the drastic changes that occur in the morphology of the precursor particles (~polycrystalline spheres) compared to the product SC-NMC particles after sintering (non-spherical particles made up of a few highly faceted crystals), it is questionable whether large precursor particles are required to make large SC-NMC; and if small submicron precursor particles might equally be used.

The above considerations make it questionable whether co-precipitation is the best process to make SC-NMC precursors or whether precursor particle morphology control is even necessary. Here we show that SC-NMC may be successfully made from

*Electrochemical Society Student Member.
**Electrochemical Society Member.
[z]E-mail: mnobrovac@dal.ca

submicron ball milled oxide precursors and, furthermore, that large (~10 μm) SC-NMC particles may be made by this method by careful control of the sintering conditions.

Experimental

Two types of NMC precursors were prepared; labelled here as precursors P1 and P2. For P1 precursor, 70 g of stoichiometric amounts of NiO powder (Sigma-Aldrich, −325 mesh, 99%), MnO powder (Aldrich, −60 mesh, 99%), and Co_3O_4 powder (Alfa Aesar, 99.7%); and 10 kg of 0.5 inch stainless steel balls were loaded into a 5 l stainless-steel jar mill (US Stoneware) and milled at 85 rpm for 1 week. For P2 precursor, 4.2 g of stoichiometric amounts of the NiO, MnO, and Co_3O_4 powders were sealed with 98 g of 1/8 inch ZrO_2 balls in a 45 ml alumina milling vial (Spex CertiPrep, Metuchen, NJ) and milled using a high energy ball mill (SPEX Model 8000-D, Spex CertiPrep, Metuchen, NJ) for 1 h. The resulting precursor powders were then collected by further milling the mixture with ethanol for another 5 min, recovering the liquid and drying. In an industrial process, where the same mill is used repeatedly for the same composition, it is anticipated that this liquid recovery/cleaning step would be unnecessary. The dried powder was ground by hand with a mortar and pestle with an amount of Li_2CO_3 (Alfa Aesar, 99%), corresponding to 10%, 15%, or 20% excess lithium content, according to the Li:Ni:Mn:Co ratio given by the formula $LiNi_{0.6}Mn_{0.2}Co_{0.2}O_2$, until a homogeneous mixture was obtained (~10 min). For SC-NMC1, SC-NMC2, and SC-NMC3, precursor P1 was used with 10%, 15%, and 20% excess lithium content, respectively, and each mixture was placed in an alumina crucible and heated in a tube furnace in air for 12 h at 940 °C. For SC-NMC4, precursor P1 was used with 20% excess lithium content, and the mixture was placed in an alumina crucible and heated in a tube furnace in flowing oxygen for 12 h at 940 °C. For SC-NMC5, precursor P2 was used with 20% excess lithium content, and the mixture was first heated in air, then ground using a mortar and pestle, and then heated again in flowing oxygen for 12 h at 940 °C. SC-NMC6 was prepared in the same way as SC-NMC5, except that the heating time in air was 24 h. Table I summarizes the synthesis conditions for the SC-NMCs made in this study. Finally, all the products were ground to fine powder by hand with mortar and pestle and passed through a 38 μm sieve.

Specific surface area was determined by the single-point Brunauer–Emmett–Teller (BET) method using a Micromeritics Flowsorb II2300 surface area analyzer. X-ray diffraction (XRD) patterns were collected using a Rigaku Ultima IV diffractometer equipped with a Cu Kα X-ray source, a diffracted beam graphite monochromator and a scintillation detector. Scanning electron microscope (SEM) images were obtained using a JEOL 840 SEM. Energy dispersive X-ray spectroscopy (EDS) mapping images were obtained using a MIRA-3 TESCAN FESEM.

Sample electrodes for laboratory testing were prepared from slurries prepared by mixing the prepared particulate, carbon black (Super C65, Imerys Graphite and Carbon), and polyvinylidene fluoride binder (PVDF, Kynar HSV 900)) in an active particle/carbon black/PVDF mass ratio of 92/4/4 with appropriate amount of N-methyl-2-pyrrolidone (NMP, Sigma Aldrich, anhydrous 99.5%). Slurries were mixed for 10 min using a high-shear mixer then spread onto aluminum foil with a 0.006 inch gap coating bar. The coatings were then dried in air for 90 min at 120 °C, punched into 1.3 cm disks and then heated under vacuum for at least 12 h at 120 °C with no further air exposure before assembling the cells. The active material loading is ~3 mg cm^{-2} (~0.6 mAh cm^{-2}).

Cell assembly was carried out in an Ar-filled glove box. Electrodes were assembled in 2325-type coin lithium half-cells with a lithium foil (99.9%, Sigma Aldrich) counter/reference electrode. Two layers of Celgard 2300 separator and one layer of blown microfiber (3 M company) were used in each coin lithium half-cell. 1 M $LiPF_6$ (BASF) in a solution of ethylene carbonate, diethyl carbonate and monofluoroethylene carbonate (volume ratio 3:6:1, all from BASF) was used as electrolyte. Cells were cycled galvanostatically with a Maccor Series 4000 Automated Test System (Maccor Inc., Tulsa OK) at 30.0 ± 0.1 °C.

Results and Discussion

Precursor structure and morphology.—Precursor P1 was made by ball milling NiO, MnO, and Co_3O_4 powders in a Ni:Mn:Co = 6:2:2 atomic ratio in a 5 l stainless steel jar mill for a week (~80 rpm). The XRD pattern of precursor P1 is shown in Fig. 1a. Precursor P1 is single-phase rock-salt with a lattice constant of 4.187 Å. The lattice constant lies within the range of the lattice constants of the constituent oxides (NiO = 4.1771 Å, MnO = 4.444 Å, CoO = 4.2612 Å), which suggests $Ni_{0.6}Mn_{0.2}Co_{0.2}O$ rock-salt solid solution formation. It is highly surprising that a single-phase rock-salt can be formed from these constituents. The lattice constants of the constituent oxide rock-salt phases all can be well predicted from crystal ionic radii (CR), assuming the commonly observed high-spin state of the 2+ ions (HS-Mn^{2+} = 0.97 Å, Ni^{2+} = 0.83, HS-Co^{2+} = 0.885 Å).[19] The radii of Ni^{2+} and Co^{2+} are within 7% of each other, therefore solid solution formation is expected for M(II) oxides of these elements. However, the HS-Mn^{2+} radius is 17% larger than HS-Ni^{2+} and is therefore not expected to be accommodated in a Ni^{2+}-rich rock-salt solid solution phase. Indeed, the predicted lattice constant of rock-salt $Ni_{0.6}Mn_{0.2}Co_{0.2}O$ using the atomic average of the high-spin ionic radii is 4.26 Å, which is much larger than the observed value of 4.187 Å. We suspect that Mn^{2+} may be forced into its smaller LS-Mn^{2+} (CR = 0.81 Å)[19] state in order for it to be accommodated in this lattice. In this case, the predicted lattice constant of the $Ni_{0.6}Mn_{0.2}Co_{0.2}O$ rock-salt phase is 4.19 Å, corresponding exactly to what is observed. Although LS-Mn^{2+} has been observed in complexes, to our knowledge it has not been observed previously in oxides, even at high pressures.[20] It may be only accessible here due to the non-equilibrium conditions encountered during ball milling. The formation of a single phase (Ni, Mn, Co)O solid solution shows that ideal atomic mixing of transition metals can be achieved by dry milling their constituent oxides. This level of mixing is highly desirable for the formation of single-phase SC-NMC product particles.

Precursor P2 was made by ball milling NiO, MnO, and Co_3O_4 powders in a Ni:Mn:Co = 6:2:2 atomic ratio for one hour in a high energy ball mill with an alumina vessel and zirconia balls. The XRD pattern of precursor P2 is shown in Fig. 1b. The precursor P2 consists of nano-grained phases of a rock-salt phase (NiO or a solid solution), MnO, and Co_3O_4. Of the phases present, the rock-salt phase has the largest grain size, which is about 19 nm, according to

Table I. Synthesis conditions of the SC-NMCs.

Sample	Precursor	Excess Li (%)	Heating Atmosphere	Heating time (h)
SC-NMC1	PM1	10	air	12
SC-NMC2	PM1	15	air	12
SC-NMC3	PM1	20	air	12
SC-NMC4	PM1	20	oxygen	12
SC-NMC5	PM2	20	air/oxygen	12/12
SC-NMC6	PM2	20	air/oxygen	24/12

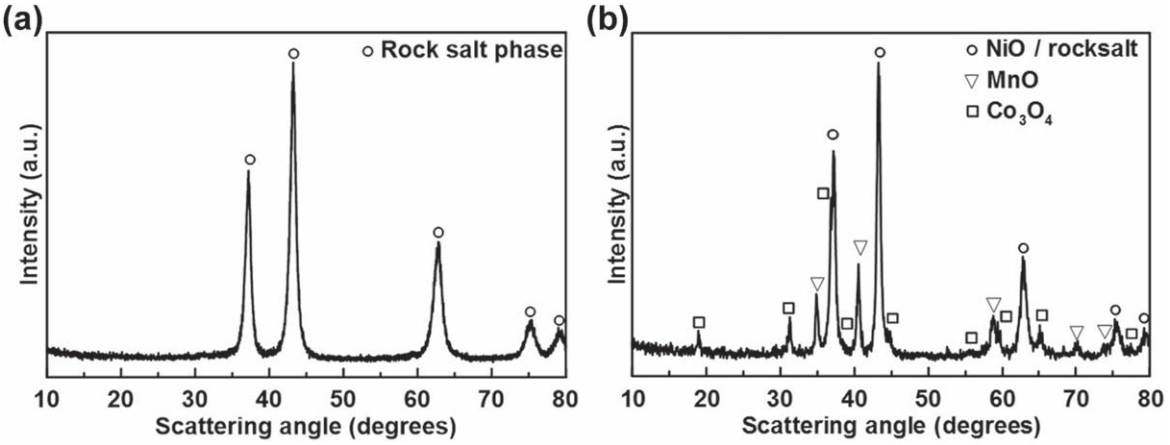

Figure 1. XRD patterns of (a) P1 and (b) P2 precursors.

the Scherrer equation. Although atomic-level mixing was not been achieved in P2, we have found that perfect atomic mixing is not necessary and single-phase SC-NMC can be formed from this precursor nonetheless. Therefore, ion diffusion during sintering is sufficient for single-phase formation even when atomic mixing is not achieved, as long as the precursor grain size is small. An SEM image of precursor P1 is shown in Fig. S2. Precursor P1 consists of loosely packed agglomerates of submicron particles. This morphology is typical of ball milled oxides. Precursor P2 has a similar morphology.

Effect of sintering conditions on SC-NMC formation.—Excess lithium salt is commonly used in the synthesis of NMC to compensate for lithium loss during high temperature sintering.[2,3] In the case of SC-NMC, adding excess lithium during synthesis also promotes the formation of single crystals.[2,3] Figure 2 shows SEM images and XRD patterns of SC-NMC synthesized by heating precursor P1 for 12 h at 940 °C in air with 10% excess lithium (a–d, SC-NMC1), 15% excess lithium (e–h, SC-NMC2), and 20% excess lithium (i–j, SC-NMC3). Larger magnification images of the three SC-NMC samples are shown in Fig. 3. All three materials have single crystal morphology with crystallite sizes in the range of 3 $\sim$ 15 μm. No impurities were observed in the XRD patterns. In the expanded XRD patterns (44°–45°), The Cu $K_{\alpha1}/K_{\alpha2}$ splitting of the (104) peak (at $\sim$44.5°) is pronounced, indicating an extremely high degree of crystallinity and large crystallite size. Figures S4a–S4c shows the XRD refinements for SC-NMC1, SC-NMC2, and SC-NMC3. For all the refinements, space group Rm (α-$NaFeO_2$ structure) was used and the lattice constants were allowed to vary. Lithium and transition metal atoms were placed at *3b* and *3a* sites, respectively. Oxygen atoms were placed at 6c sites (0, 0, $\times$), where

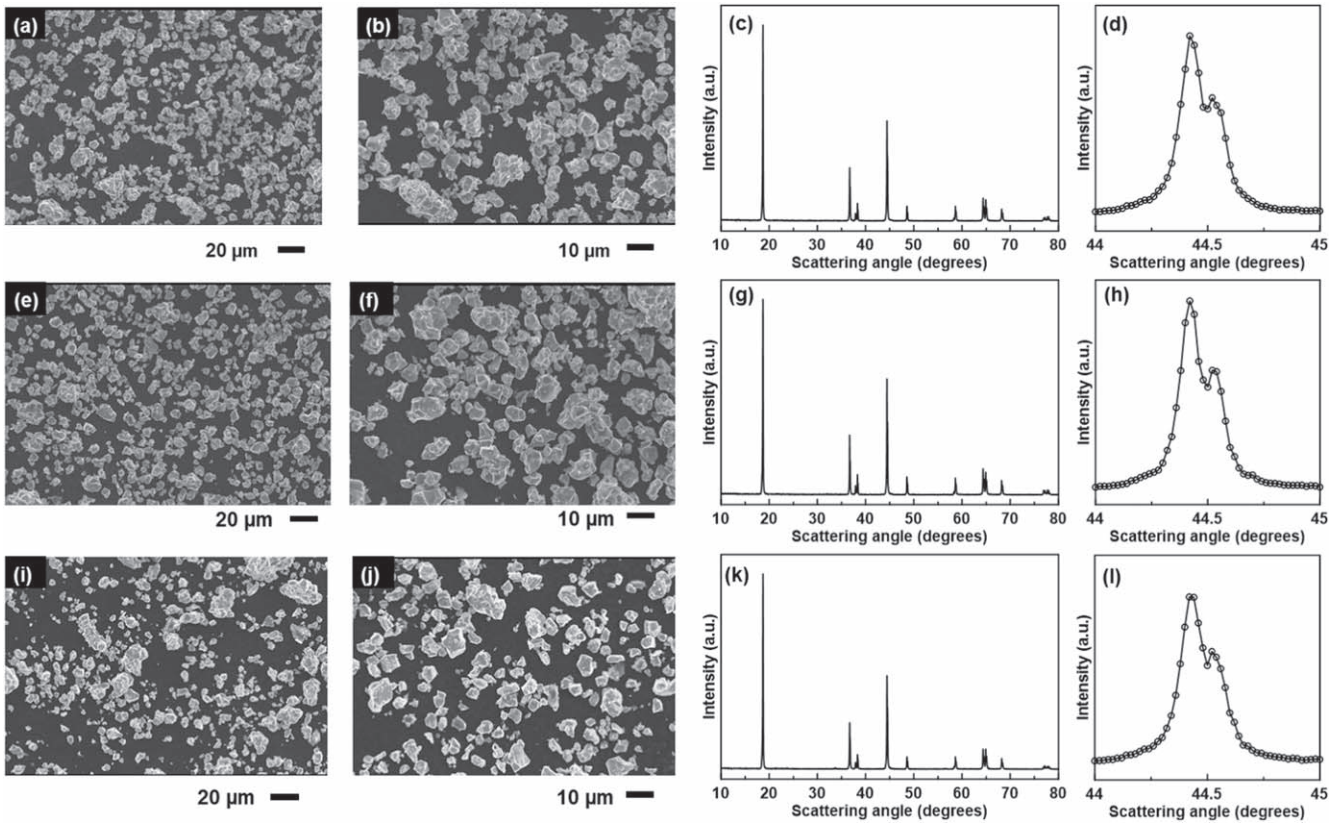

Figure 2. SEM images and XRD patterns of (a)–(d) SC-NMC1, (e)–(h) SC-NMC2, and (i)–(l) SC-NMC3.

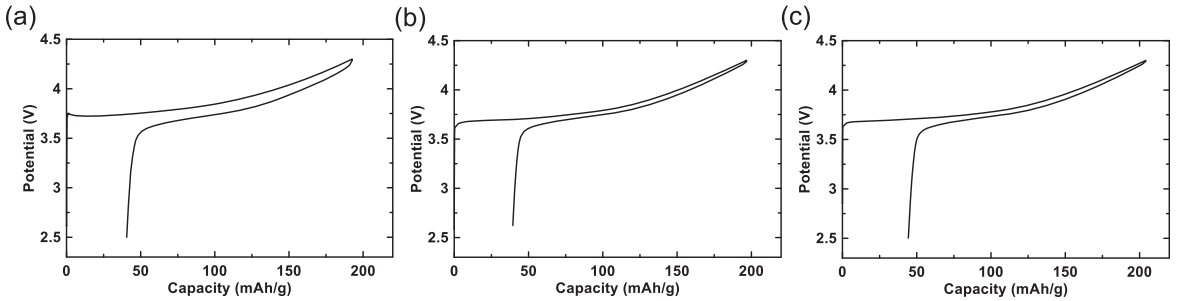

Figure 3. First cycle potential profiles of (a) SC-NMC1, (b) SC-NMC2, and (c) SC-NMC3.

x was initially 0.26 and was allowed to vary during the fit. Cation mixing between lithium and nickel was also allowed in the refinement. Table SII summarizes the refinement results. A relatively high degree (~3%) of cation mixing between Ni and Li was observed for SC-NMC1, SC-NMC2, and SC-NMC3. Cation mixing in these layered oxides is known to cause polarization.

Figure 3 shows the potential profiles of SC-NMC1-3. The first cycle charge capacity increases as excess lithium content increases. When cycled between 2.5−4.3 V at C/20 (10 mA g^{-1}), each SC-NMC shows a first cycle charge capacity of 193 mAh g^{-1}, 196 mAh g^{-1}, and 204 mAh g^{-1}, respectively. SC-NMC1, the sample with the highest amount of cation mixing, also has the highest polarization, as would be expected. The smaller polarization of SC-NMC2 and SC-NMC3, shows the beneficial effect of adding more excess lithium. However, the high first cycle irreversible capacity (~20%) for all 3 materials is not satisfactory.

It is known that for NMC cathodes with high nickel content, heating in oxygen results in better performance, as oxygen ensures sufficient oxidation of nickel, reducing Ni^{2+}/Li^{+} mixing.[21] Figure 4 shows SEM images (a, b), XRD patterns (c, d), and the potential profile (e) of P1 precursor mixed with 20% excess lithium carbonate and heated for 12 h at 940 °C in oxygen (SC-NMC4). A higher magnification SEM image is shown in Fig. S5. SC-NMC4 is composed of crystallites having an average size of 1–2 μm. The crystallite size is significantly smaller than SC-NMC1, SC-NMC2, and SC-NMC3, which indicates heating in oxygen does not promote crystallite growth, compared to heating in air. This can also be seen in the XRD pattern. A shoulder on the right side of the (104) peak (at ~44.5°) can be observed, while no clear Cu $K_{\alpha1}/K_{\alpha2}$ peak splitting can be observed, as shown in Fig. 4c, indicating the degree of crystallinity is not as high as SC-NMC1, SC-NMC2, and SC-NMC3. Figure 4d shows the first cycle potential profile of SC-NMC4. When cycled between 2.5 − 4.3 V at C/20 (10 mA g^{-1}), a reversible capacity of ~165 mAh g^{-1} with an irreversible capacity of ~31 mAh g^{-1} can be obtained. Notably, the first cycle coulombic efficiency is ~85%, significantly better than SC-NMC1, SC-NMC2, and SC-NMC3. However, more optimization is still required to further improve the coulombic efficiency and increase the crystallite size.

SC-NMC from ball-milled precursors using a 2-step sintering process.—From the previous section we learned that while heating in oxygen gives better electrochemical performance, the obtained crystallite size is small, which is not desirable, as it can lead to particle cracking, and increased surface reactions with electrolyte.

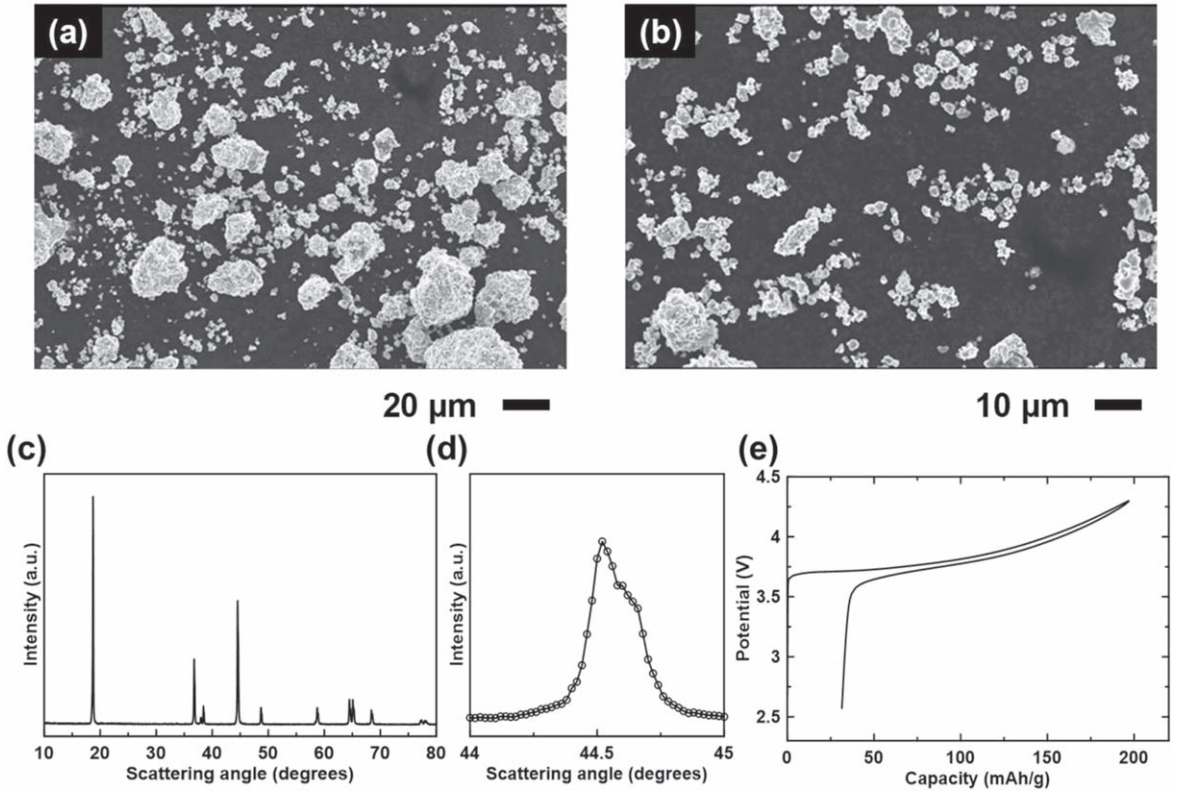

Figure 4. (a), (b) SEM images, (c), (d) XRD patterns, and (e) first cycle potential profile of SC-NMC4.

On the other hand, heating in air results in larger primary particle size, at the expense of an inferior electrochemistry due to cation mixing. We therefore developed a 2-step sintering method in which the precursor mixture was first heated in air to promote the crystal growth. The heated sample was then ground and reheated in oxygen to reduce cation mixing and enhance electrochemical performance. We also used iron-free milling conditions (P2 precursor), to prevent any iron contamination in the resulting sample. Figures 5a–5c shows SEM images and EDS maps of the resulting SC-NMC synthesized using the 2-step air/oxygen heating method (SC-NMC5). A higher magnification SEM image is shown in Fig. S6. SC-NMC5 is composed of single crystals, 3 $\sim$ 10 μm in size. A homogeneous distribution of Ni, Mn, and Co can be observed in the EDS maps. The crystallites have clear facets, resulting in a low BET surface area of 0.57 $m^2\ g^{-1}$. The morphology and size of SC-NMC5 are similar to previous reports where co-precipitation precursors were used.[3,9] Figures 5d–5f shows an XRD pattern of SC-NMC5. It is phase pure and has very narrow peak widths, corresponding to the instrumental broadening error (0.11°). The splitting of the (104) peak (at ~44.5°) is pronounced, as shown in Fig. 5f, indicating an extremely high degree of crystallinity, which is characteristic of single crystal NMC materials. Figures S3d–S3e shows the Rietveld refinements for SC-NMC4 and SC-NMC5. Refinement results are summarized in Table II. According to the refinement, the Li/Ni cation mixing was 1.83% and 1.99%, respectively, for SC-NMC4 and SC-NMC5, confirming that oxygen heating reduces the cation mixing while the large crystallite size was maintained during the heating step. These properties could contribute to a higher first cycle coulombic efficiency.

Table II. XRD refinement results for the SC-NMCs.

Sample	a (Å)	c (Å)	Ni_{Li}%	Bragg R-factor
SC-NMC1	2.871	14.231	3.22	5.35
SC-NMC2	2.871	14.230	2.69	3.81
SC-NMC3	2.869	14.221	3.00	3.52
SC-NMC4	2.862	14.207	1.83	3.36
SC-NMC5	2.863	14.212	1.99	3.83

Figure 6a shows the first cycle potential profile of SC-NMC5. When cycled between 2.5−4.3 V at C/20 (10 mA g^{-1}), SC-NMC5 has a first cycle reversible capacity of ~162 mAh g^{-1} and a first cycle irreversible capacity of ~24 mAh g^{-1} (87% first cycle coulombic efficiency). The second cycle average polarization is only 0.09 V. Figure 6b shows the cycling performance of SC at a current rate of C/5. After 90 cycles ~90% of capacity was retained. This potential profile, first cycle coulombic efficiency, and capacity retention is comparable with SC-NMC materials reported by other researchers that used co-precipitated precursors.[3,22] Figure S7 shows

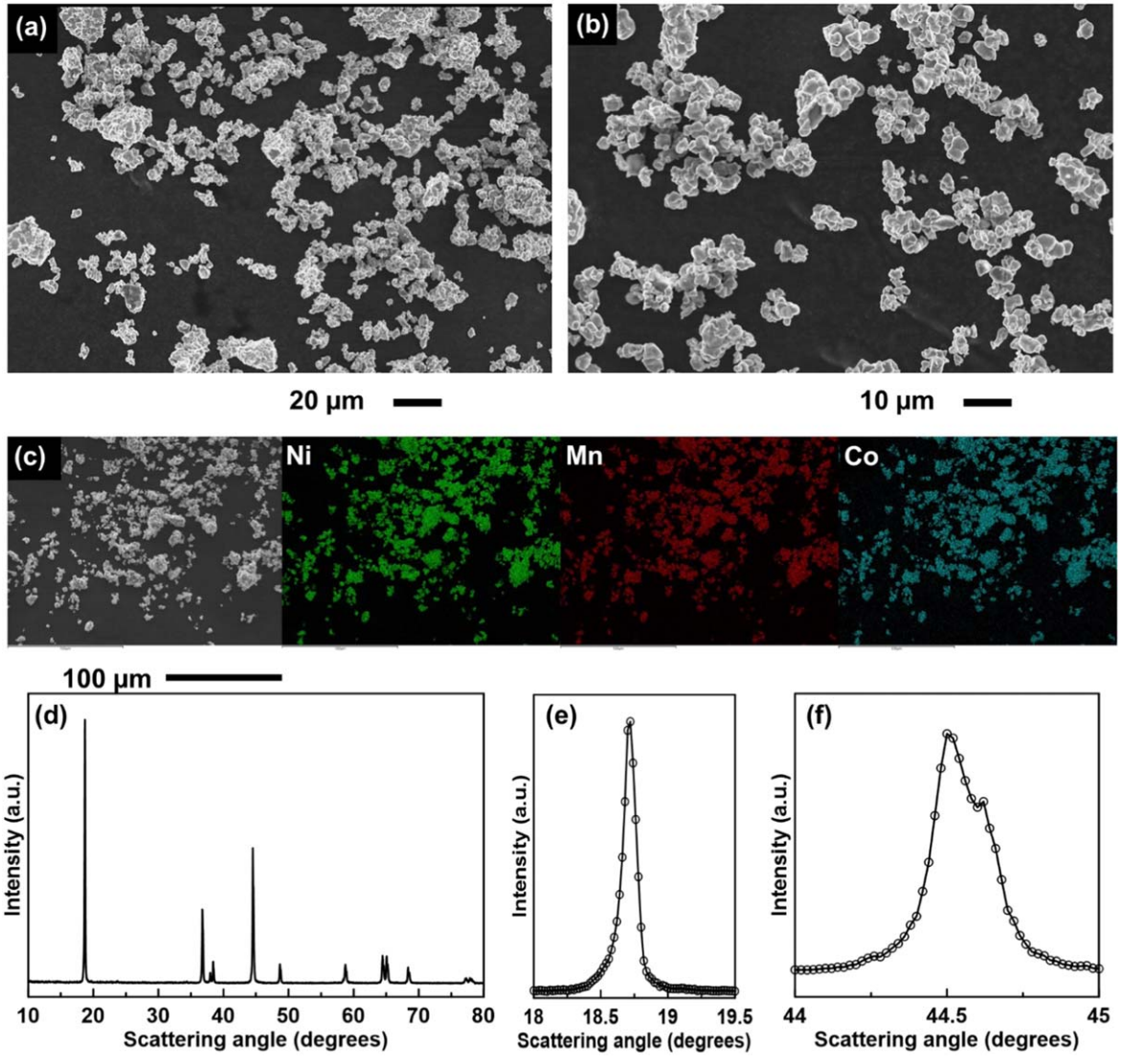

Figure 5. (a)–(b) SEM images, (c) EDS elemental maps of Ni, Mn, and Co, and (d)–(f) XRD patterns of SC-NMC5.

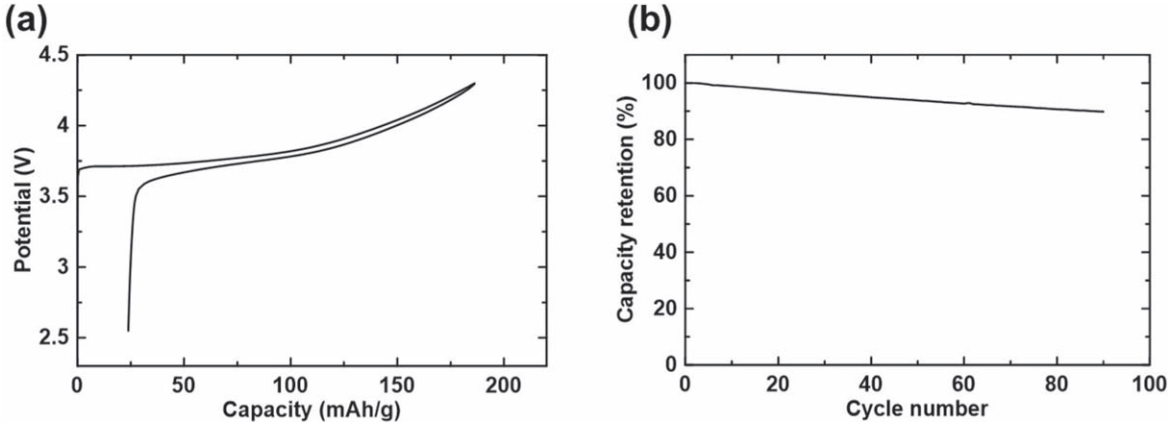

Figure 6. (a) First cycle potential profile and (b) cycling performance of SC-NMC5.

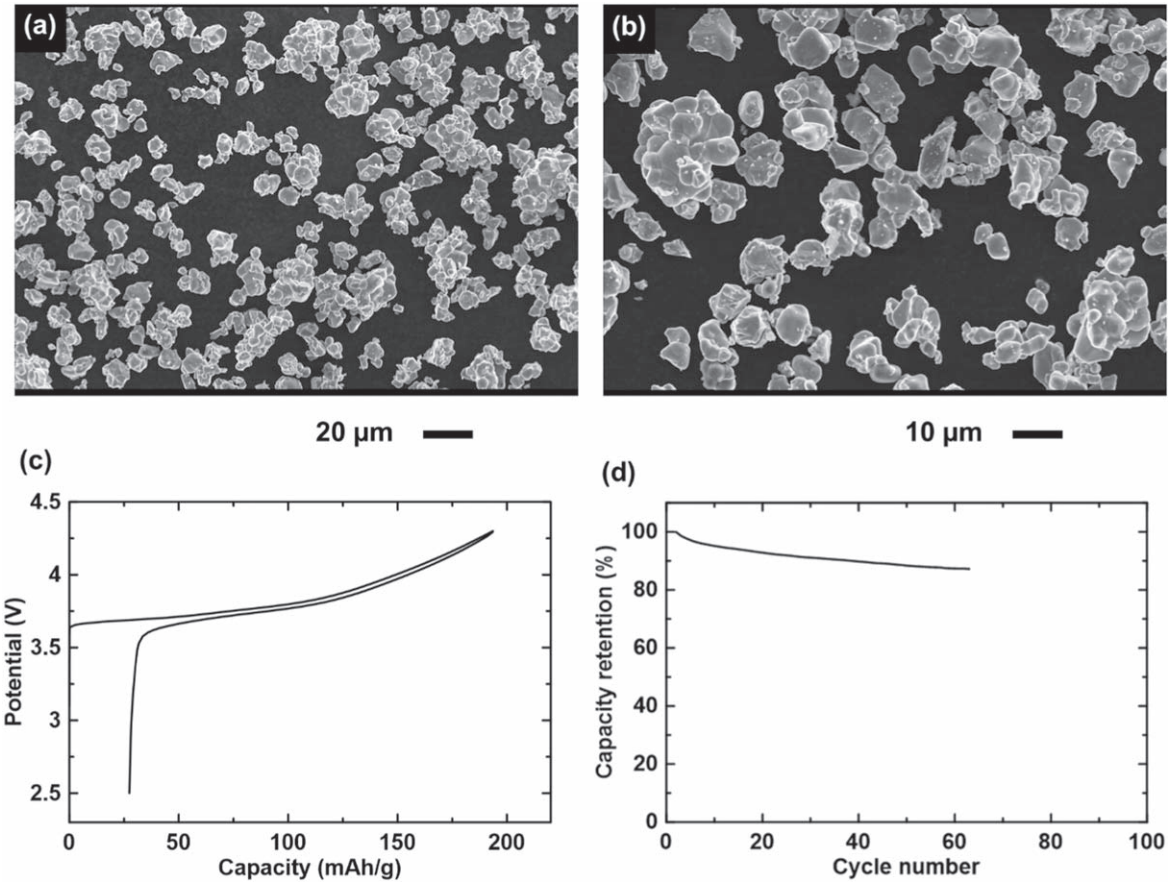

Figure 7. (a)–(b) SEM images of large SC-NMC synthesized using all-dry method by extending heating time. (c) First cycle voltage curve and (d) cycling performance of large SC-NMC.

the specific capacity vs cycle number for the SC-NMCs. While SC-NMC5 shows decent cycling performance, other SC-NMCs have rapid capacity fading during cycling. Elemental analysis was conducted using EDX to compare the chemical composition of samples prepared from the two different precursors. The results are listed in Table SI. The material made from P1 precursor (SC-NMC3) has slight iron contamination, while material made from P2 precursor (SC-NMC5) has slight aluminum contamination, both in the range of 3–4 atomic%. Other possible elements, such as Cr and Zr, were not detected. These impurity elements are likely to be doped into the surface or bulk structure of the materials and can affect the electrochemistry. For example, small amount of iron doping has been shown to deteriorate the electrochemical performance of NMC, while small amount of aluminum doping can enhance the cycling performance.[23] These might contribute to the superior performance of SC-NMC5 than the rest materials made from P1 precursor. The rate performance of SC-NMC5 is shown in Fig. S8. At 1 C current rate (200 mA g^{-1}), more than half of the capacity is retained for SC-NMC5. The rate capability is slightly inferior than SC-NMC reported before made using co-precipitated precursor.[3] More studies are required to further improve the rate performance.

Since a large excess of lithium was used during the synthesis, it is likely that excess residual lithium compounds, such as LiOH or Li_2CO_3 exist on the surface of the particles. This can lead to air-sensitivity, low capacity, and low first cycle efficiency. The

performance of this material is expected to be improved by optimizing the synthesis conditions and post treatments, such as washing/reheating.[24] Further improvements may be made by methods widely used in industry, such as elemental doping, surface coating, electrolyte additives, etc.[22,25–28] Nevertheless, it was thought previously, that the particle size of the co-precipitated precursor governs the SC-NMC crystallite size.[29] Here we show that this is not the case. Instead, the size of SC-NMC can be easily controlled by varying the heating time in air. As shown in Figs. 7a–7d, larger SC-NMC (SC-NMC6) can be made by simply extending the heating time in air from 12 to 24 h, even when precursors with submicron particle sizes are used. While this paper only aims to introduce the new method of synthesis with early results, the most favorable heating conditions (time, temperature, atmosphere) regarding the cost, safety, electrochemical performance need to be further studied in detail.

Conclusions

In summary, we have developed an all-dry method for producing single crystal lithium cathode materials with a layered structure. This method was developed from the following key discoveries:

- Ball milling a mixture of transition metal oxides can produce homogeneous Ni,Mn,Co-oxide precursors, even to the extent of atomic mixing, so that previously unobserved (Ni, Mn, Co) O solid solution rock salt phase precursors can be formed.
- The final crystallite size of SC-NMC is only related to the heating conditions and has no relation to the precursor particle size, as previously believed.
- A large crystallite size SC-NMC with low cation mixing can be achieved from ball milled precursors using a 2-step air/O_2 sintering.

Using an all dry method instead of co-precipitation to synthesize precursors for SC cathode materials has significant implications. As reviewed in the introduction, the environmental benefits of an all dry method are apparent: it has high yield, produces little waste, and saves large amounts of water. Compared to the co-precipitation process, the dry process is significantly less complicated, as compared in Fig. S1. Such a large reduction in processing steps is typically associated with lower cost. Another advantage with the all-dry method is that the choices of precursors can be more flexible than the co-precipitation method, as for the dry process they need not be soluble, nor are they required to precipitate at the same pH. It is expected this method can be applied to make other SC cathode materials, including $LiNi_xCo_yAl_zO_2$ (NCA), cobalt-free layered cathodes, or layered cathode materials with special dopants, such as W, Mo, etc., possibly enabling materials not accessible by the co-precipitation method. We therefore hope to expand the use of these dry processing methods in future studies.

ORCID

M. N. Obrovac https://orcid.org/0000-0001-5509-3185

References

1. G. E. Blomgren, *J. Electrochem. Soc.*, **164**, A5019 (2017).
2. J. Li, A. R. Cameron, H. Li, S. Glazier, D. Xiong, M. Chatzidakis, J. Allen, G. A. Botton, and J. R. Dahn, *J. Electrochem. Soc.*, **164**, A1534 (2017).
3. H. Li, J. Li, X. Ma, and J. R. Dahn, *J. Electrochem. Soc.*, **165**, A1038 (2018).
4. Z. Zhong, L. Chen, S. Huang, W. Shang, L. Kong, M. Sun, L. Chen, and W. Ren, *J. Mater. Sci.*, **55**, 2913 (2020).
5. H.-H. Ryu, K.-J. Park, C. S. Yoon, and Y.-K. Sun, *Chem. Mater.*, **30**, 1155 (2018).
6. H.-H. Sun and A. Manthiram, *Chem. Mater.*, **29**, 8486 (2017).
7. H.-J. Noh, S. Youn, C. S. Yoon, and Y.-K. Sun, *J. Power Sources*, **233**, 121 (2013).
8. G. Qian et al., *Energy Storage Mater.*, **27**, 140 (2020).
9. J. E. Harlow et al., *J. Electrochem. Soc.*, **166**, A3031 (2019).
10. F. Zhou, X. Zhao, A. van Bommel, A. W. Rowe, and J. R. Dahn, *Chem. Mater.*, **22**, 1015 (2010).
11. D. Wang, I. Belharouak, L. H. Ortega, X. Zhang, R. Xu, D. Zhou, G. Zhou, and K. Amine, *J. Power Sources*, **274**, 451 (2015).
12. S. Ahmed, P. A. Nelson, K. G. Gallagher, N. Susarla, and D. W. Dees, *J. Power Sources*, **342**, 733 (2017).
13. A. Liu and J. Dahn, *ChemEngineering*, **3**, 38 (2019).
14. G.-T. Park, H.-H. Ryu, N.-Y. Park, C. S. Yoon, and Y.-K. Sun, *J. Power Sources*, **442**, 227242 (2019).
15. N. Kosova, N. F. Uvarov, E. T. Devyatkina, and E. G. Avvakumov, *Solid State Ionics*, **135**, 107 (2000).
16. M. N. Obrovac, O. Mao, and J. R. Dahn, *Solid State Ionics*, **112**, 9 (1998).
17. M. N. Obrovac, L. Zheng, and M. D. L. Garayt, *Cell Reports Physical Science*, **1**, 100063 (2020).
18. W. Yan, J. Jiang, W. Liu, X. Yan, D. Sun, Y. Jin, J. Wang, L. Xiang, H. Munakata, and K. Kanamura, *Electrochim. Acta*, **212**, 16 (2016).
19. R. D. Shannon, *Acta Crystallogr., Sect. A*, **A32**, 751 (1976).
20. D. M. Sherman, *Am. Mineral.*, **69**, 788 (1984).
21. J.-H. Shim, C.-Y. Kim, S.-W. Cho, A. Missiul, J.-K. Kim, Y. J. Ahn, and S. Lee, *Electrochim. Acta*, **138**, 15 (2014).
22. B. Huang, X. Yang, G. Xu, M. Wang, and Y. Gu, *Ionics*, **25**, 5819 (2019).
23. D. Liu, Z. Wang, and L. Chen, *Electrochim. Acta*, **51**, 4199 (2006).
24. X. Xiong, Z. Wang, P. Yue, H. Guo, F. Wu, J. Wang, and X. Li, *J. Power Sources*, **222**, 318 (2013).
25. L. Zheng, C. Wei, M. D. L. Garayt, J. MacInnis, and M. N. Obrovac, *J. Electrochem. Soc.*, **166**, A2924 (2019).
26. L. Zheng, T. D. Hatchard, and M. N. Obrovac, *MRC*, **9**, 245 (2019).
27. Y. Lu, X. Zeng, J. Wang, L. Yang, S. Hu, C. Jia, H. Zhao, D. Yin, X. Ge, and X. Xi, *Adv. Mater. Interfaces*, **6**, 1901368 (2019).
28. E. R. Logan, H. Hebecker, X. Ma, J. Quinn, Y. HyeJeong, S. Kumakura, J. Paulsen, and J. R. Dahn, *J. Electrochem. Soc.*, **167**, 060530 (2020).
29. J. Li, H. Li, W. Stone, R. Weber, S. Hy, and J. R. Dahn, *J. Electrochem. Soc.*, **164**, A3529 (2017).